

ASCA Observation of the Low-Luminosity Seyfert 1.5 Galaxy

NGC 5033

Yuichi TERASHIMA*, Hideyo KUNIEDA, and Kazutami MISAKI

Department of Physics, Nagoya University, Chikusa-ku, Nagoya 464-8602

(Received 1998 October 8; accepted 1999 February 23)

Abstract

We present the results of an ASCA observation of the low-luminosity Seyfert 1.5 galaxy NGC 5033. A point-like X-ray source with a luminosity of 2.3×10^{41} erg s $^{-1}$ in the 2–10 keV band (at 18.7 Mpc; Tully 1988, AAA045.002.054) was detected at the nucleus. The X-ray light curve shows variability on a timescale of $\sim 10^4$ s with an amplitude of $\sim 20\%$. The X-ray continuum is represented by a weakly absorbed ($N_{\text{H}} \approx 9 \times 10^{20}$ cm $^{-2}$) power-law with a photon index of 1.72 ± 0.04 , which is quite similar to Seyfert 1 galaxies with higher luminosities. A Fe K α emission line is detected at $6.40_{-0.06}^{+0.08}$ keV (redshift corrected) and the equivalent width is 290 ± 100 eV. The line width is unresolved. The narrower line width and larger equivalent width compared to Seyfert 1s imply that fluorescent Fe K α emission from matter further out from the center than the accretion disk significantly contributes to the observed Fe K α line. We suggest that fluorescent Fe K α emission from the putative torus contributes to the observed Fe K α line.

Key words: Galaxies: active — Galaxies: individual (NGC 5033) — Galaxies: Seyfert — X-Rays: spectra

* Present address: NASA Goddard Space Flight Center, Code 662, Greenbelt, MD 20771, USA.

1. Introduction

Extensive studies of nearby galactic nuclei established that many nearby galaxies harbor low-luminosity active galactic nuclei (LLAGNs) (Ho 1999; Ho et al. 1997a, b). In the X-ray regime, their luminosities are typically $10^{40} - 10^{41}$ erg s $^{-1}$ in the energy range of 2–10 keV. X-ray observations of such AGNs provide us with a good opportunity to study the accretion and emission mechanisms of AGNs under extremely low-luminosity conditions. Owing to the high sensitivity and imaging capability at energies above 2 keV of the ASCA satellite (Tanaka et al. 1994), several LLAGNs have been detected (Makishima et al. 1994; Ptak et al. 1996; Ishisaki et al. 1996; Iyomoto et al. 1996, 1997, 1998; Serlemitsos et al. 1996; Nicholson et al. 1998; Terashima et al. 1998a, b). ASCA observations have revealed that the X-ray continuum shape in LLAGNs is quite similar to that of luminous Seyfert galaxies in spite of their low luminosity. On the other hand, the LLAGNs M81 and NGC 4579 show higher center energies of the Fe K α emission, which are consistent with He-like Fe (Ishisaki et al. 1996; Serlemitsos et al. 1996; Terashima et al. 1998b), while no Fe K α emission is detected from NGC 1097 (Iyomoto et al. 1996), NGC 3065, and NGC 4203 (Iyomoto et al. 1998). These Fe K α emission-line properties are different from that of Seyfert galaxies, in which broad Fe K α emission is generally detected at ~ 6.4 keV (e.g. Nandra et al. 1997b). Furthermore, LLAGNs do not show any rapid and large-amplitude variability, in contrast to Seyfert galaxies (Ishisaki et al. 1996; Iyomoto et al. 1996, 1998; Terashima et al. 1998b; Ptak et al. 1998; Awaki et al. in preparation). In regular Seyfert 1 galaxies, lower luminosity objects tend to show variability with large amplitude on short timescales (Nandra et al. 1997a; Mushotzky et al. 1993). Such differences between LLAGNs and Seyfert 1s have been attributed to the difference in the structure of the accretion disks (Ptak et al. 1998) or the central black-hole mass (Awaki et al. in preparation). Further X-ray observations of LLAGNs are of great importance to investigate these differences between LLAGNs and ‘classical’ AGNs in order to understand the underlying physics in LLAGNs,

NGC 5033 is a nearby (18.7 Mpc, $z = 0.00292$; Tully 1988; we use a value of $H_0 = 75$ km s $^{-1}$ Mpc $^{-1}$ for the Hubble constant) SBc galaxy with a Seyfert nucleus. The H α and H β emission lines have strong, broad components, leading to the classification of NGC 5033 as a Seyfert 1.5 galaxy. The broad

$\text{H}\alpha$ emission line is variable (Ho et al. 1997a, b; Koratkar et al. 1995; Filippenko, Sargent 1985; Stauffer 1982). The narrow $\text{H}\alpha$ luminosity is only $\log L(\text{H}\alpha) = 39.32$ (here L in erg s^{-1}), which is smaller than the well-studied low-luminosity Seyfert galaxy NGC 4051.

X-ray observations of NGC 5033 have been performed with various instruments (Polletta et al. 1996 and references therein). In the soft X-ray band, Einstein IPC detected an X-ray source at the nucleus (Halpern, Steiner 1983), and the X-ray emission is unresolved in a ROSAT HRI image (Koratkar et al. 1995). Although there are a few hard X-ray observations above 2 keV, no spectral information has been obtained so far. For example, EXOSAT detected X-ray emission with a flux of $4.7 \times 10^{-12} \text{ erg s}^{-1} \text{ cm}^{-2}$ in the 2–10 keV band, but the X-ray spectral shape is not constrained because of limited photon statistics and background systematics (Turner, Pounds 1989).

In this paper, we report on the first measurements of an X-ray spectrum and the detection of Fe $\text{K}\alpha$ emission.

2. Observation

We observed NGC 5033 with ASCA on 1995 December 14. A detailed description of the ASCA instruments can be found in Serlemitsos et al. (1995), Ohashi et al. (1996), Makishima et al. (1996), Burke et al. (1994), and Yamashita et al. (1997). The Solid-state Imaging Spectrometers (SIS 0 and SIS 1) were operated in 1 CCD FAINT mode. The Gas Imaging Spectrometers (GIS 2 and GIS 3) were operated in the PH normal mode. We obtained net exposure times of 36 ks and 39 ks for SIS and GIS, respectively, after standard data screening. X-ray spectra and light curves were extracted from circular regions centered on the NGC 5033 nucleus with a radius of 4' for SIS and 6' for GIS. The spectra from SIS 0 and SIS 1 were combined after gain corrections. The spectra from GIS 2 and GIS 3 were also combined. Background data were accumulated from a source-free region in the same field. The mean count rates for SIS and GIS were 0.16 c s^{-1} and 0.11 c s^{-1} per detector, respectively, after background subtraction.

3. Results

An X-ray source is clearly detected at the position of the NGC 5033 nucleus within the accuracy of the position determination. Significant X-ray variability is seen in all instruments. The combined X-ray light curve of the SIS (0.5–10 keV) + GIS (0.7–10 keV) data with a bin size of 5760 s (one orbit of the ASCA satellite) is shown in figure 1. Intensity variations of $\sim 20\%$ on timescales of $\sim 10^4$ s are clearly seen. A constant model fit to this light curve yields $\chi^2=106$ for 14 degrees of freedom. We calculated a normalized excess variance, as defined in Nandra et al. (1997a), using a light curve obtained with SIS 0+1 in the 0.5–10 keV band with a bin size of 128 s, and obtained $\sigma_{\text{rms}}^2 = (1.7 \pm 0.7) \times 10^{-3}$.

The X-ray spectra obtained with SIS and GIS are shown in figure 2. The X-ray continuum is well represented by a single power-law modified by photoelectric absorption, and an emission-line feature is seen at around 6.4 keV. Therefore, we fit the overall spectra with an absorbed power-law continuum plus a Gaussian model. This model provides a good fit to the data ($\chi^2_{\nu} = 0.93$ for 188 dof), and the best-fit parameters are summarized in table 1., where the line is assumed to have zero width. The best-fit model is shown as a histogram in figure 2. The photon index is 1.72 ± 0.04 and the absorption column density ($N_{\text{H}} = 8.7 \pm 1.7 \times 10^{20} \text{ cm}^{-2}$) is slightly higher than the galactic value of $1.1 \times 10^{20} \text{ cm}^{-2}$ (Murphy et al. 1996) (hereafter the quoted errors are at the 90% confidence level for one interesting parameter). The X-ray flux in the 2–10 keV band is $5.5 \times 10^{-12} \text{ erg s}^{-1} \text{ cm}^{-2}$, which corresponds to $2.3 \times 10^{41} \text{ erg s}^{-1}$ at a distance of 18.7 Mpc. The error for the flux is $\sim 10\%$, which is dominated by calibration uncertainties. The addition of a Gaussian line to a power-law continuum model significantly improved the χ^2 value by $\Delta\chi^2 = -22.5$ for two additional parameters (line center energy and intensity). According to the *F*-test, this component is statistically significant at 99.999% confidence. The best-fit line center energy and equivalent width are $6.38_{-0.06}^{+0.08} \text{ keV}$ (observed frame) and $290 \pm 100 \text{ eV}$, respectively. This line centroid energy indicates that the origin of the emission is fluorescence from cold iron. If the line width is allowed to vary, the χ^2 value improves by only $\Delta\chi^2 = -0.4$ and the line center, width, and equivalent width become $6.41_{-0.09}^{+0.14} \text{ keV}$, $100_{-100}^{+160} \text{ eV}$, and $320_{-140}^{+110} \text{ eV}$, respectively. Thus, the line is unresolved. The upper limit of the line width, $\sigma \approx 260 \text{ eV}$, corresponds to $\sigma \approx 12000 \text{ km s}^{-1}$. The spectrum around the Fe K α

emission is shown in figure 3 as ratios of the data to the best-fit continuum model. Confidence contours for the line energy versus intensity and for the line width versus intensity are shown in figures 4 and 5, respectively. The low energy (red) side of the profile is steep, in contrast to the line profiles typical of Seyfert 1 galaxies, which have an extended red wing (e.g. Nandra et al. 1997b). The Fe line profile indicates a hint of a wing at higher energies from the peak. However, the addition of a second, Gaussian line at 6.7 keV gives no significant improvement in the fit ($\Delta\chi^2 = -2.0$).

Many Seyfert 1 galaxies show an Fe K α line profile skewed to lower energies. This is interpreted in terms of the origin of the line in the innermost part of an accretion disk (e.g. Tanaka et al. 1995; Nandra et al. 1997b). We also apply the disk-line model (Fabian et al. 1989) to the Fe K α emission from NGC 5033. Since the photon statistics are limited, we fix the line center energy at 6.4 keV and the inner radius of the line emitting region at $6r_g$, where $r_g = GM/c^2$ is the gravitational radius. The line emissivity is assumed to be proportional to r^{-q} and q is fixed at 2.5, which is a typical value for Seyfert 1 galaxies (Nandra et al. 1997b). In this model fit, the outer radius of the line emitting region becomes greater than $1000r_g$, indicating that the Fe line is mainly emitted from an extended region in which relativistic effects are not significant and that the line width is relatively narrow. This is consistent with the Gaussian-fit result described above. Additionally, the observed line profile shows no significant red asymmetry. We tentatively fixed the outer radius at $1000r_g$ and obtained a slightly worse fit ($\chi^2=179.4$ for 188 dof) than the Gaussian model. The best-fit inclination angle and equivalent width are $37^{\circ+13}_{-11}$ and $490^{\pm220}_{-210}$ eV, respectively. The results of various model fits to the Fe K α line are summarized in table 2.

A thermal bremsstrahlung plus Gaussian model was also tried, but provided a worse χ^2 ($\Delta\chi^2 = +25.5$) than the power-law plus Gaussian fit, and systematic negative and positive residuals are seen below 0.7 keV and above 7 keV, respectively. Furthermore, the best-fit center energy of the Gaussian component, 6.40 keV (redshift corrected), indicates that the emission line is due to fluorescence from neutral or low ionization-state (<Fe XVI) iron. We therefore conclude that a thermal model is not appropriate for the NGC 5033 spectrum.

Finally, we searched for the variability of the Fe K line intensity within the observation. We

extracted the X-ray counts using the first 40.7 ks and the last 46.1 ks of the observation yielding spectra in a low- and high-flux state, respectively. These spectra were fitted with a power-law plus Gaussian model, where the line was assumed to have zero width. The fitting results are also summarized in table 1. No significant Fe K α line variability was detected between these two spectra. The X-ray fluxes in the 2–10 keV band are 5.0×10^{-12} erg s $^{-1}$ cm $^{-2}$ and 6.0×10^{-12} erg s $^{-1}$ cm $^{-2}$, for low- and high-flux state, respectively. The statistical errors (including the uncertainties in the spectral fits) of these X-ray fluxes are $\sim 4\%$, which are valid for comparisons between the datasets analyzed here. The uncertainties for the absolute fluxes are $\sim 10\%$.

4. Discussion

4.1. X-Ray Variability

We detected X-ray emission with a luminosity of 2.3×10^{41} erg s $^{-1}$ from the nucleus of NGC 5033. X-ray variability on timescales of $\sim 10^4$ s was detected in a one day observation, and the observed variability amplitude was only $\sim 20\%$. Since less luminous Seyfert 1 galaxies tend to show large amplitude and rapid variability compared to luminous Seyfert 1 and quasars (Nandra et al. 1997a; Lawrence, Papadakis 1993), the observed variability amplitude is smaller than that expected from this trend. The normalized excess variance, $\sigma_{\text{rms}}^2 = 1.7 \times 10^{-3}$, is about two orders of magnitude smaller than the relation between σ_{rms} and the X-ray luminosities for the Seyfert 1 galaxies reported in Nandra et al. (1997a) and similar to other LLAGNs (Ptak et al. 1998).

The small-amplitude variability could be explained if hard X-ray emitting components besides an AGN, such as X-ray binaries and starburst activity, contribute to the X-ray flux significantly. Then, the AGN component would be diluted, leading to a smaller observed amplitude variability than that intrinsic to the AGN X-ray emission. However, this possibility seems to be unlikely for the following reasons. In normal spiral galaxies, X-ray emission mainly comes from the superposition of discrete sources, such as low-mass X-ray binaries, and the X-ray luminosity is roughly proportional to the B-band luminosities L_B (e.g. Fabbiano 1989). The large L_X/L_B ratio ($L_X/L_B = 1.5 \times 10^{-3}$) for NGC 5033 compared to

that of normal spiral galaxies (e.g. $L_X/L_B = 3.5 \times 10^{-5}$ for M31; Makishima et al. 1989) combined with the poor fit to the thermal model characteristic of low mass X-ray binaries suggests that the emission from X-ray binaries does not contribute to the X-ray flux significantly. Also, there is no evidence for the soft thermal X-ray emission of $kT \sim 1$ keV which accompanies starburst activity in the host galaxy (e.g. Tsuru et al. 1997; Moran, Lehnert 1997; Ptak et al. 1997). Additionally, the X-ray continuum of NGC 5033 is well represented by a power-law, and thermal bremsstrahlung emission does not fit the data, which appear to be present in the X-ray spectrum of starburst galaxies (e.g. $kT \sim 6$ keV for NGC 253, Persic et al. 1998). We conclude that the observed small amplitude of the variation is an intrinsic property of the AGN in NGC 5033.

NGC 5033 also shares the variability characteristics of previously observed LLAGNs, and we confirmed that little or no variability is quite common in low-luminosity AGNs with X-ray luminosities $<\sim 10^{41}$ erg s $^{-1}$, as suggested in Ptak et al. (1998) and Awaki et al. (in preparation). We note that the low-luminosity Seyfert 1 NGC 4051 (e.g. $L_X \sim 8 \times 10^{41}$ erg s $^{-1}$ at 17 Mpc; Guainazzi et al. 1996), which is known to show rapid and large-amplitude X-ray variability, is most likely to be a narrow-line Seyfert 1 galaxy (Ho et al. 1997b; Osterbrock, Pogge 1985), which is a subclass of Seyfert galaxies often showing rapid X-ray variability (e.g. Boller et al. 1996). Thus, the negative correlation between the amplitudes and luminosities is no longer seen at luminosities below $\sim 10^{41}$ erg s $^{-1}$.

4.2. X-Ray Continuum

The X-ray spectrum of NGC 5033 is well represented by the combination of a power-law continuum and a Gaussian line. The continuum is fitted by a power-law with a photon index of $\Gamma = 1.72 \pm 0.04$, which is very similar to Seyfert 1 galaxies with higher luminosities (Nandra et al. 1997b). In Seyfert 1 galaxies, intrinsic photon indices are steeper ($\Gamma \approx 1.9$) than observed if the effect of Compton reflection is taken into account. In the case of NGC 5033, the intrinsic photon index cannot be constrained because of the limited photon statistics and energy bandpass. The detection of strong, fluorescent Fe K α emission implies that the reflection component due to cold matter, which produces the Fe emission, is present. It is thus likely that the intrinsic photon index in NGC 5033 is steeper than that observed, and is also

consistent with higher luminosity Seyfert 1 galaxies. Thus, we do not find any evidence for a luminosity dependence of the X-ray continuum slope.

4.3. *Fe K α Emission*

We detected an Fe K α emission line at 6.4 keV which is due to fluorescence in cold iron. The detection of Fe K α from several LLAGNs has been reported. Although strong fluorescent Fe K α is detected from LLAGNs with large intrinsic absorption ($N_{\text{H}} > 10^{23} \text{ cm}^{-2}$) (Makishima et al. 1994; Terashima et al. 1998a; Maiolino et al. 1998), this is the first LLAGN with small intrinsic absorption to show an Fe K α emission line at 6.4 keV. Since other LLAGNs with small intrinsic absorption show no Fe K α emission (NGC 1097; Iyomoto et al. 1997) or an Fe K α line at ~ 6.7 keV (M81 Ishisaki et al. 1996; Serlemitos et al. 1996; NGC 4579 Terashima et al. 1998b), we conclude that a variety of center energies and equivalent widths of Fe lines is observed in LLAGNs.

An Fe K α line peaking at 6.4 keV is generally observed from Seyfert 1 galaxies, and the line width is often observed to be broad and skewed to lower energies (Nandra et al. 1997b). Such Fe K α emission from Seyfert 1 galaxies is interpreted as originating in the innermost part of an accretion disk (e.g. Tanaka et al. 1995). The Fe K α line in NGC 5033 is unresolved, and no clear signature of the profile skewed to lower energies is seen. Moreover, the equivalent width, 290 ± 100 eV, is larger than the equivalent width of the narrow core of the Fe lines in Seyfert 1 galaxies (100–150 eV) (Nandra et al. 1997b). These results suggest that the narrow fluorescent Fe K α line emission from beyond the accretion disk, possibly the putative molecular torus assumed in the unified scheme, contributes to the observed Fe emission. Note that the Fe line profiles of Seyfert 1 galaxies are well fitted with the disk-line model by Fabian et al. (1989) and only a weak additional narrow component is required in all but a small number of objects (Nandra et al. 1997b). The torus out of the line of sight could be absent or subtend a small solid angle viewed from the nucleus in Seyfert 1 galaxies.

Variability of the Fe K α line intensity has been detected in several bright Seyfert 1 galaxies on timescales of less than one day (Iwasawa et al. 1996; Yaqoob et al. 1996; Nandra et al. 1997c). Such variability also supports that Fe K α emission comes from the inner part (< one light day) of the

accretion disk. On the other hand, no significant intensity variability has been observed within the one-day observation of NGC 5033, although the photon statistics are limited. This is consistent with the picture that the Fe $K\alpha$ in NGC 5033 is produced mainly in the putative torus.

Thus, the relatively narrow and strong Fe $K\alpha$ line in NGC 5033 can be explained if a narrow Fe line from the torus significantly contributes to the observed Fe emission. The optical emission line widths of NGC 5033 classify it as an intermediate type (Seyfert 1.5). This intermediate classification might also be explained if we are seeing the central engine from an intermediate inclination angle and the broad line region is partly obscured. Then, the inner surface of the torus can account for the fluorescent Fe emission. Thus, we suggest that the obscuring torus assumed in the unified scheme of Seyfert galaxies is present around the central engine of NGC 5033 in contrast to Seyfert 1 galaxies, in which the torus contribution to Fe $K\alpha$ emission is not important (Nandra et al. 1997a), possibly because the torus is absent or subtends a small solid angle viewed from the nucleus.

Future spectroscopic observations with higher energy resolution should be able to decompose the broad (diskline) and narrow (outer part of the accretion disk and/or putative torus) components.

The authors thank T. Yaqoob for a critical reading of the manuscript, and all of the ASCA team members who made this study possible. YT and KM thank JSPS for support.

References

Boller Th., Brandt W.N., Fink H. 1996, A&A 305 53
Burke B.E., Mountain R.W., Daniels P.J., Dolat V.S. 1994, IEEE Trans. NS-41, 375
Fabbiano G. 1989, ARA&A 27, 87
Fabian A.C., Rees M.J., Stella L., White N.E. 1989, MNRAS 238, 729
Filippenko A.V., Sargent W.L.W. 1985, ApJS 57, 503
Guainazzi M., Mihara T., Otani C., Matsuoka M. 1996, PASJ 48, 781
Halpern J.P., Steiner J.E. 1983, ApJ 269, L37
Ho L.C. 1999, in The 32nd COSPAR meeting, The AGN-Galaxy connection (Advances in Space

Research, Oxford), in press

Ho L.C., Filippenko A.V., Sargent W.L.W. 1997a, ApJS 112, 315

Ho L.C., Filippenko A.V., Sargent W.L.W., Peng C.Y. 1997b, ApJS 112, 391

Ishisaki Y., Makishima K., Iyomoto N., Hayashida K., Inoue H., Mitsuda K., Tanaka Y., Uno S. et al. 1996, PASJ 48, 237

Iwasawa K., Fabian A.C., Reynolds C.S., Nandra K., Otani C., Inoue H., Hayashida K., Brandt W.N. et al. 1996, MNRAS 282, 1038

Iyomoto N., Makishima K., Fukazawa Y., Tashiro M., Ishisaki Y. 1997, PASJ 49, 425

Iyomoto, N. Makishima, K. Fukazawa, Y. Tashiro, M., Ishisaki Y. Nakai N., Taniguchi Y. 1996, PASJ 48, 231

Iyomoto N., Makishima K., Matsushita K., Fukazawa Y., Tashiro M., Ohashi T. 1998, ApJ 503, 168

Koratkar A., Deustua S.E., Heckman T., Filippenko A.V., Ho L.C., Rao M. 1995, ApJ 440, 132
Lawrence A., Papadakis I. 1993, ApJ 414, L85

Maiolino R., Salvati M., Bassani L., Dadina M., Della Ceca R., Matt G., Risaliti G., Zamorani G. 1998, A&A 338, 781

Makishima K., Fujimoto R., Ishisaki Y., Kii T., Loewenstein M., Mushotzky R., Serlemitsos P., Sonobe T. et al. 1994, PASJ 46, L77

Makishima K., Ohashi T., Hayashida K., Inoue H., Koyama K., Takano S., Tanaka Y., Yoshida A. et al. 1989, PASJ 41, 697

Makishima K., Tashiro M., Ebisawa K., Ezawa H., Fukazawa Y., Gunji S., Hirayama M., Idesawa E. et al. 1996, PASJ 48, 171

Moran E.C., Lehnert M.D. 1997, ApJ 478, 172

Murphy E.M., Lockman F.J., Laor A., Elvis M. 1996, ApJS 105, 369

Mushotzky R.F., Done, C., Pounds K.A. 1993, ARA&A 31, 717

Nandra K., George I.M., Mushotzky R.F., Turner T.J., Yaqoob T. 1997a, ApJ 476, 70

Nandra K., George I.M., Mushotzky R.F., Turner T.J., Yaqoob T 1997b, ApJ 477, 602

Nandra K., George I.M., Mushotzky R.F., Turner T.J., Yaqoob T 1997c, MNRAS 284, L7

Nicholson K.L., Reichert G.A., Mason K.O., Puchnarewicz E.M., Ho L.C., Shields J.C., Filippenko A.V. 1998, MNRAS 300, 893

Ohashi T., Ebisawa K., Fukazawa Y., Hiyoshi K., Horii M., Ikebe Y., Ikeda H., Inoue H. et al. 1996, PASJ 48, 157

Osterbrock D.E., Pogge R.W. 1985, ApJ 297, 166

Persic M., Mariani S., Cappi M., Bassani L., Danese L., Dean A.J., Di Cocco G., Franceschini A. et al. A&A 339, L33

Polletta, M., Bassani, L., Malaguti, G., Palumbo, G.G.C., Caroli, E. 1996, ApJS 106, 399

Ptak A., Serlemitsos P., Yaqoob T., Mushotzky R., Tsuru T. 1997, AJ 113, 1286

Ptak A., Yaqoob T., Mushotzky R., Serlemitsos P., Griffiths R. 1998, ApJ 501, L37

Ptak A., Yaqoob T., Serlemitsos P.J., Kunieda H., Terashima Y. 1996, ApJ 459, 542

Serlemitsos P.J., Jalota L., Soong Y., Kunieda H., Tawara Y., Tsusaka Y., Suzuki H., Sakima Y. et al. 1995, PASJ 47, 105

Serlemitsos P.J., Ptak A.F., Yaqoob T. 1996, in The Physics of LINERs in View of Recent Observations, ed. Eracleous M., Koratkar A., Leitherer C., Ho L.C. (ASP, San Francisco) p70

Stauffer J.R. 1982, ApJ 262, 66

Tanaka Y., Inoue H., Holt S.S. 1994, PASJ 46, L37

Tanaka Y., Nandra K., Fabian A.C., Inoue H., Otani C., Dotani T., Hayashida K., Iwasawa K. et al 1995, Nature 375, 659

Terashima Y., Kunieda H., Misaki K., Mushotzky R.F., Ptak A.F., Reichert G.A. 1998b, ApJ 503, 212

Terashima Y., Ptak A.F., Fujimoto R., Itoh M., Kunieda H., Makishima K. Serlemitsos P.J. 1998a, ApJ 496, 210

Tsuru T., Awaki H., Koyama K., Ptak A. 1997, PASJ 49, 619

Tully R.B. 1988, Nearby Galaxies Catalog, (Cambridge Univ. Press: Cambridge)

Turner T.J., Pounds K.A 1989, MNRAS 240, 833

Yamashita A., Dotani T., Bautz M., Crew G., Ezuka H., Gendreau K., Kotani T., Mitsuda K.

et al. 1997, IEEE Trans. NS-44, 847

Yaqoob T., Serlemitsos P.J., Turner T.J., George I.M., Nandra K. 1996, ApJ 470, L27

Table 1. Results of spectral fits to the SIS and GIS spectra of NGC 5033.*

	N_{H} [10^{20} cm^{-2}]	Photon index	Energy [keV]	EW [eV]	χ^2/dof
Total	8.7 ± 1.7	1.72 ± 0.04	$6.38_{-0.06}^{+0.08}$	290 ± 100	174.0/188
Low	9.0 ± 1.7	1.77 ± 0.07	$6.30_{-0.09}^{+0.13}$	350_{-160}^{+150}	167.5/166
High	8.8 ± 2.4	1.72 ± 0.06	6.48 ± 0.12	300_{-140}^{+170}	202.1/198

* Line widths are assumed to have zero width. Line energies are in the observed frame.

Table 2. Model fits to the Fe K line.*

Model	Energy [keV]	σ [eV] or inclination [deg]	EW [eV]	χ^2/dof
(1) Narrow	$6.38_{-0.06}^{+0.08}$	0	290 ± 100	174.0/188
Gaussian line				
(2) Broad	$6.41_{-0.09}^{+0.14}$	100_{-100}^{+160}	320_{-140}^{+110}	173.6/187
Gaussian line .				
(3) Two	$6.36_{-0.06}^{+0.07}$	0	260_{-120}^{+100}	172.0/187
narrow				
Gaussian lines	6.68	0	90_{-90}^{+140}	
(4) Disk-line .	6.38	37_{-11}^{+13}	490_{-210}^{+220}	179.4/188

* The values without errors are frozen parameters. Line energies are in the observed frame.

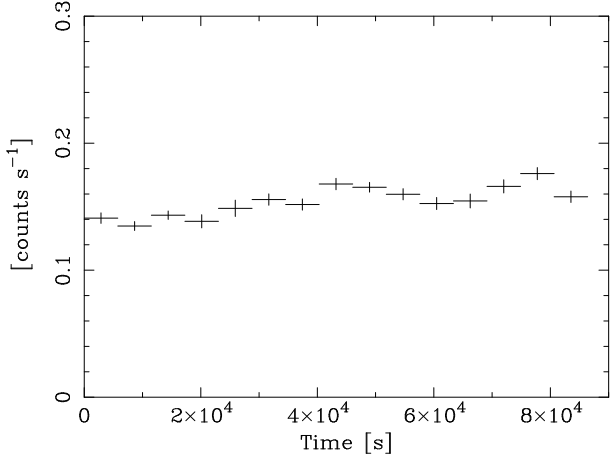


Fig. 1.. X-ray light curve of NGC 5033. SIS (0.5–10 keV) and GIS (0.7–10 keV) data are combined.
Bin size = 5760 s (one orbital period of the ASCA satellite).

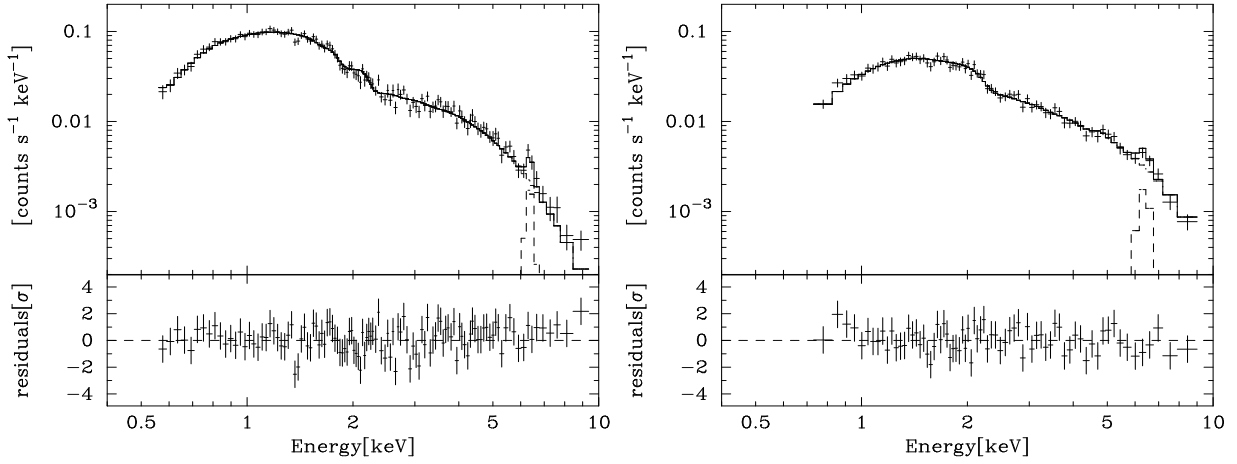


Fig. 2.. X-ray spectra of NGC 5033. left: SIS, right: GIS. Though spectral fits are done simultaneously, the figures are shown separately for clarity. The histograms indicate the best-fit power-law plus Gaussian model.

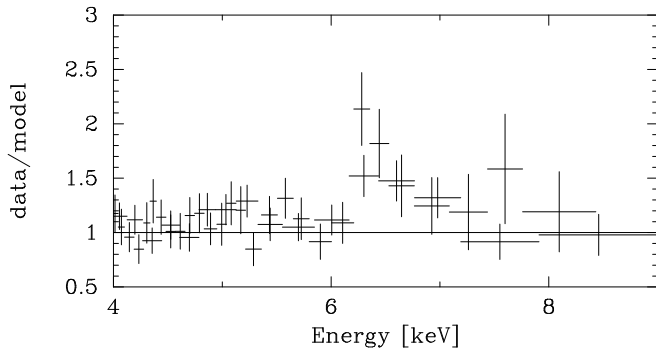


Fig. 3.. Data/model ratios around Fe K α emission in NGC 5033. The energy scale is not redshift corrected.

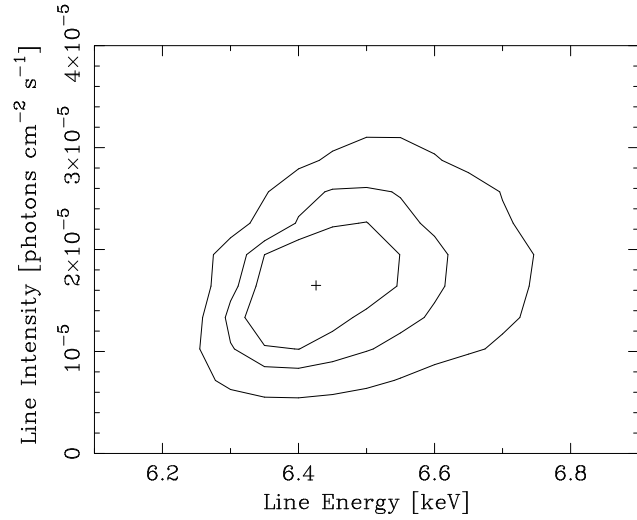


Fig. 4.. Confidence contours for the line energy and intensity. The line width is left to vary. The contours correspond to 68, 90, and 99% confidence level for two interesting parameters ($\Delta\chi^2 = 2.3$, 4.6, and 9.2, respectively). The energy scale is not red shift corrected.

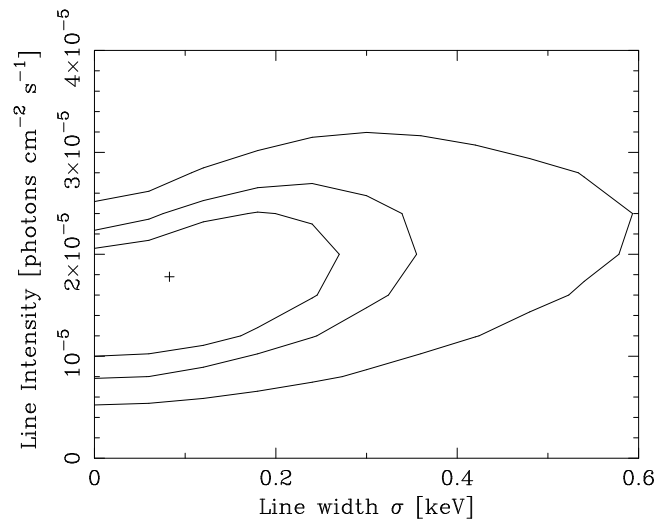


Fig. 5.. Confidence contours for the line width and intensity. The contours correspond to 68, 90, and 99% confidence level for two interesting parameters ($\Delta\chi^2 = 2.3, 4.6$, and 9.2 , respectively).